Precision Medicine and Imaging

Clinical Cancer Research

# Multiplexed (18-Plex) Measurement of Signaling Targets and Cytotoxic T Cells in Trastuzumab-Treated Patients using Imaging Mass Cytometry

Daniel E. Carvajal-Hausdorf[1,2], Jonathan Patsenker[1,3], Kelly P. Stanton[1], Franz Villarroel-Espindola[1], Amanda Esch[4], Ruth R. Montgomery[1], Amanda Psyrri[5], Konstantine T. Kalogeras[6], Vassiliki Kotoula[7], George Foutzilas[8], Kurt A. Schalper[1], Yuval Kluger[1], and David L. Rimm[1]

## Abstract

**Purpose:** Imaging mass cytometry (IMC) uses metal-conjugated antibodies to provide multidimensional, objective measurement of protein targets. We used this high-throughput platform to perform an 18-plex assessment of HER2 ICD/ECD, cytotoxic T-cell infiltration and other structural and signaling proteins in a cohort of patients treated with trastuzumab to discover associations with trastuzumab benefit.

**Experimental Design:** An antibody panel for detection of 18 targets (pan-cytokeratin, HER2 ICD, HER2 ECD, CD8, vimentin, cytokeratin 7, β-catenin, HER3, MET, EGFR, ERK 1–2, MEK 1–2, PTEN, PI3K p110 α, Akt, mTOR, Ki67, and Histone H3) was used with a selection of trastuzumab-treated patients from the Hellenic Cooperative Oncology Group 10/05 trial ($n = 180$), and identified a case–control series.

**Results:** Patients that recurred after adjuvant treatment with trastuzumab trended toward a decreased fraction of HER2 ECD pixels over threshold compared with cases without recurrence ($P = 0.057$). After exclusion of the lowest HER2 expressers, 5-year recurrence events were associated with reduced total extracellular domain (ECD)/intracellular domain (ICD) ratio intensity in tumor ($P = 0.044$). These observations are consistent with our previous work using quantitative immunofluorescence, but represent the proof on identical cell content. We also describe the association of the ECD of HER2 with CD8 T-cell infiltration on the same slide.

**Conclusions:** The proximity of CD8 cells as a function of the expression of the ECD of HER2 provides further evidence for the role of the immune system in the mechanism of action of trastuzumab.

## Introduction

Trastuzumab, a therapeutic antibody directed against the extracellular domain (ECD) of HER2 has been postulated to work both by inhibition of the tyrosine kinase activity (1) of the HER2 protein and by antibody-dependent cell toxicity (2, 3). These data are largely derived from mechanistic studies in model systems but the role of each of these mechanisms in patient with breast cancer tumors is not completely understood. It has also been observed that HER2 is activated by homo- or heterodimerization with other ERBB family members (1) and can be processed by the cleavage of ECD (4). The role of the p95 cytoplasmic domain fragment has been studied and there is some evidence that its presence is associated with lack of response to trastuzumab because this molecule contains the tyrosine kinase activity but not the trastuzumab-binding site in the ECD. Although efforts were made to use antibodies to the p95 fragment to detect trastuzumab resistance, these antibodies were never able to successfully prove the mechanism. On the basis of this same concept, we found that quantitative-independent measurement of both the extracellular and intracellular domain (ICD) of HER2 could identify differential benefit from adjuvant (5) and neoadjuvant (6) trastuzumab treatment. These findings were obtained using serial sections of tissue for each target and are being further tested on tissue from the ALTTO trial (7). However, existing methods did not allow concurrent analysis of the role of the immune system in the therapeutic effect. Thus, we sought a high-plex method that would allow simultaneous assessment of immune cells, along with both domains of the HER2 protein and downstream proteins associated with HER2 signaling, all on the same tissue section.

Traditional methods for *in situ* protein assessment of molecular biomarkers in solid tumors can maximally detect 7–8 targets in formalin-fixed, paraffin embedded (FFPE) tissues (8–13). However, practically, to accurately measure targets in this context, some of the fluorophore channels need to be used for phenotyping or compartmentalization, thereby limiting the number of targets that can be measured to 3 or 4. Furthermore, the quantum yield and detection capabilities make quantitative comparisons between channels challenging. While consecutive sections may be used, these suffer from heterogeneity issues, especially with respect to measurements of the microenvironment. Approaches

[1]Yale School of Medicine, New Haven, Connecticut. [2]Clínica Alemana-Facultad de Medicina U. del Desarrollo, Santiago, Chile. [3]Rensselaer Polytechnic Institute, Troy, New York. [4]Fluidigm Corporation, Markham, Ontario, Canada. [5]Attikon University Hospital, Athens, Greece. [6]Translational Research Section, Hellenic Cooperative Oncology Group, Athens, Greece. [7]Aristotle University of Thessaloniki School of Medicine, Thessaloniki, Greece. [8]Department of Medical Oncology, "Papageorgiou" Hospital, Athens, Greece.

**Note:** Supplementary data for this article are available at Clinical Cancer Research Online (http://clincancerres.aacrjournals.org/).

**Corresponding Author:** David L. Rimm, Yale School of Medicine, PO Box 208023, 310 Cedar Street, New Haven, CT 06520-8023. Phone: 203-737-4204; E-mail: david.rimm@yale.edu

**doi:** 10.1158/1078-0432.CCR-18-2599

## Translational Relevance

High multiplicity *in situ* assessment of protein expression, done by imaging mass cytometry (IMC), allows simultaneous measurement of many proteins on a single-histology slide. By examining 18 variables at once, we first confirmed the findings seen by fluorescent multiplexing (and validating the IMC method) showing that breast cancer tumors that do not express the ECD of the HER2 protein are less likely to benefit from trastuzumab. Then, using one of the targets included in the highly multiplexed panel, we show spatial association between $CD8^+$ T cells and the ECD of HER2. This association is consistent with the hypothesized role for antibody-dependent cell cytotoxicity postulated as a mechanism of action for trastuzumab.

based on cyclic immunofluorescence (IF; ref. 14) have been proposed as an alternative for highly multiplexed *in situ* proteomic analysis. More than 50 antigens can be detected using sequential staining and peroxide-based quenching of dyes. Recently, Lin and colleagues (15) provided a comprehensive quantitative study of the effect of cyclic staining over tissue quality and antigenicity. While reagents and analytic equipment required are readily available, significant issues remain with tissue and antigen loss over cycles, commercial antibodies being not compatible with the process and signal changes. While very promising, the technology has not shown equivalence of measurement of a continuous antigen in cycle 1 compared with cycle 10 or more. This limitation may be unimportant for some issues, but more important for others.

Two technologies have been developed that promise to extend the ability to quantitatively assess and range of proteins on a single-tissue section. Both work using heavy metal–conjugated antibodies that are ionized from the surface of the tissue slide. Imaging mass cytometry (IMC; ref. 16), combines laser ablation in argon followed by time-of-flight mass spectrometry, while multiplexed ion beam imaging (17) uses an ion beam ablation under vacuum combined with time-of-flight mass spectrometry. Both have enabled the simultaneous detection of over 50 molecules with subcellular resolution and creation of images with high resolution based on mapping the metal labels back to the pixel from which they were ablated. Here, we use the IMC method in tissue from patients with breast cancer to simultaneously assess the immune microenvironment and 18 proteins related to HER2 signaling. Our studies specifically probe the role of the extracellular domain of HER2 and a proposed mechanism of action of trastuzumab.

## Materials and Methods

### Antibodies and immunofluorescent staining

Eighteen commercial mAbs (Supplementary Table S1) were conjugated to unique metals (16, 18) using Maxpar Metal Labeling Kits (Fluidigm Corp.) according to the manufacturer's instructions. Tagged antibodies were then used to stain breast cancer, lung cancer, and melanoma tissue microarrays (TMA), as described previously (5). These included negative and positive controls, and cases with a range of expression for each marker. Briefly, fresh TMA cuts were deparaffinized at 60°C for 20 minutes, then incubated twice in xylene for 20 minutes. Antigen retrieval was performed with EDTA buffer pH 8.0 at 97°C for 20 minutes in a pretreatment heating device (PT Module, Lab Vision, Thermo Fisher Scientific). Endogenous peroxidase activity was blocked with 2.5% hydroxyl peroxide in methanol for 30 minutes, followed by blocking with 0.3% BSA in 0.1 mol/L of TBS for 30 minutes at room temperature. TMA sections were incubated overnight at 4°C with each primary antibody and a polyclonal rabbit anti-cow pan-cytokeratin antibody (1:100, Z0622, Dako), or a monoclonal mouse anti-human cytokeratin antibody (1:100, clone AE1/AE3, Dako). Sections were then incubated for 1 hour at room temperature with Alexa 546–conjugated goat anti-rabbit secondary antibody (Molecular Probes) diluted 1:100 in mouse EnVision Amplification Reagent (Dako), or Alexa 546–conjugated goat anti-mouse secondary antibody (Molecular Probes) in 1:100 rabbit Envision Amplification Reagent (Dako). Cyanine 5 directly conjugated to tyramide (PerkinElmer) at 1:50 dilution was used for target antibody detection. ProLong Mounting Medium (ProLong Gold, Molecular Probes) with 4,6-diamidino-2-phenylindole (DAPI) was used to stain nuclei.

### Fluorescent measurement and scoring

Quantitative IF (QIF) was performed using the AQUA (Navigate BioPharma Inc.) method (19, 20). Briefly, the QIF scores were calculated by dividing the target compartment pixel intensities by the area of cytokeratin positivity or by the area of absence of cytokeratin positivity with an expanded DAPI compartment, respectively. QIF scores were normalized to the exposure time and bit depth at which the images were captured, allowing scores collected at different exposure times to be comparable. All acquired histospots were visually evaluated and cases with staining artifacts or less than 1% tumor (cytokeratin staining) were excluded from the analysis.

### Antibody titration and validation

To optimize the titer for each conjugated antibody, we stained the standardization TMAs using at least four or five concentrations covering more than one order of magnitude in serial sections. Titration curves for each antibody using the average scores were plotted. We calculated the average of the highest 10% and lowest 10% of spots, their difference, and ratio (Supplementary Fig. S1). We defined objectively the optimal antibody titer as the one that had the highest dynamic range of signal with a specific pattern of staining as described previously (21).

Each antibody was validated in the manner described previously (22, 23) including nine of the 18 antibodies that had been previously validated in earlier work. To confirm that the conjugated metal did not affect the interaction with antigen, all antibodies were validated with the IMC platform by comparing metal-labeled antibody to unlabeled antibody using QIF on index arrays (see Supplementary Fig. S2).

### Breast cancer cohort

The Hellenic Cooperative Oncology Group (HeCOG) 10/05 trial (5, 24) was a sequential, dose-dense, three-arm breast cancer adjuvant study performed between July 2005 and November 2008, including 990 patients randomized to epirubicin, paclitaxel, and cyclophosphamide, methotrexate, and fluorouracil (CMF), compared with epirubicin, CMF, and either weekly paclitaxel or docetaxel. $HER2^+$ patients ($n = 180$) received sequentially 1 year of trastuzumab. We extracted the information and

subjected histospots to analysis from all patients that presented with recurrences before 5 years ($n = 20$) and 41 control patients matched by age and stage. The clinico-pathologic characteristics of this series are presented in Supplementary Table S2.

### Labeling for IMC

Conjugated antibodies were used to label TMA slides containing histospots from the case–control series of trastuzumab-treated patients. Briefly, fresh TMA cuts were deparaffinized at 60°C for 20 minutes, then incubated twice in xylene for 20 minutes. Antigen retrieval was performed with EDTA buffer pH 8.0 at 97°C for 20 minutes in a pretreatment heating container (PT Module, Thermo Fisher Scientific). Then, slides were blocked with 0.3% BSA in 0.1 mol/L of TBS for 30 minutes at room temperature. TMA sections were incubated overnight at 4°C with 18 tagged, primary antibodies (Supplementary Table S1). After labeling, slides were rinsed in phosphate buffer solution, and air-dried.

### IMC procedure

Selected histospots were subjected to automated ablation using an argon-based laser in the Hyperion Imaging System (Fluidigm). Tissues were laser ablated in a rastering pattern at 200 Hz and the aerosol containing the ion cloud was directly transported to a Helios Mass Cytometer (Fluidigm; refs. 16, 18). The data were exported to a .txt file with counts for each metal for each pixel. TMA spots represent 350,000–500,000 pixels each. All raw data were analyzed using locally designed Python routines (Python Software Foundation) to study molecular distribution, marker intensity, and colocalization at a pixel (1 $\mu m^2$) level.

### Noise determination

To define the signal from background for each metal we assessed the frequency distribution of pixel intensity where each antibody/metal combination showed a recognizable, specific pattern of staining. Using cytokeratin as a reference we determined the minima of the first curve as a cut-point, where all signal levels above the cut-point are defined as signal and below the cut-point are background (Supplementary Fig. S3A). This method was automated and applied to analysis of tumor expression of HER2 ICD and ECD and intratumoral CD8 levels with respect to recurrence status and geographic analysis. Extension of this method to intratumoral CD8 levels was less robust. As an alternative, for each marker we retained only the highest expressing pixels above a percentile threshold; we used the 95th percentile for cytokeratin (CK), ICD, and ECD, and 99th percentile for CD8 (Supplementary Fig. S3B). The latter method was used for geographic analysis.

### Pixel-based analysis and geographic analysis

While segmentation of images has been used with previous IMC work (18), here we attempted to assess expression with a pixel colocalization approach independent of heuristic-based fractionation of the image into trained operator-defined regions. This approach is similar in concept to the AQUA method of QIF (19). For comparison with recurrence status, we used the previously described method of noise determination and calculated the fraction of HER ECD pixels present in a compartment thresholded for CK and then HER2 ICD. Using the same approach in a smaller subset of patients, we defined the CK compartment and ratioed ECD and ICD intensities. Finally, we calculated the survival for the groups stratified by the median for ECD/ICD in the CK compartment, using Kaplan–Meier estimator and log-rank test.

To achieve spatially informed analysis and determine the contours of the tumor, a Gaussian blur (using the scipy.ndimage python module with sigma = 19) was applied to the denoised HER2 ICD image (keeping the measurements of ICD above the 95th percentile of expression), and a threshold (0.5) was chosen. All pixels with values above the threshold were compartmentalized into tumor (value "1"), and all below, to nontumor (value "0"). As an alternative, we also applied the GrabCut algorithm from the image processing cv2 python module, to create the same tumor contours, which produced similar results. To create perimeter and envelope images, inwards and outwards dilations of 10 μm were performed by applying a dilation approach on the binary images. The white perimeter (see Fig. 5A) was created by using a dilation with a $3 \times 3$ Euclidian kernel on the binary image (pixels within the tumor region were set to 1, and those outside of the region to 0). The output of the dilation represents the Euclidian distance from each pixel within the tumor to the closest boundary of the tumor in μm. This inward perimeter is defined by the pixels where the dilation output had a value $x$ μm, where $0<x\leq10$. Each green and blue envelope (see Fig. 5A) was created by taking a dilation on the image, with a $3 \times 3$ Euclidean kernel (pixels within the tumor region were set to 0, and those outside of the region to 1). The output of the dilation represents the distance from each pixel outside the tumor to the closest boundary of the tumor in μm. The first envelope is defined by the pixels where the dilation output value is $x$, such that $0<x\leq10$. Similarly the nine subsequent envelopes are determined by pixels with output values $x$, where $10<x\leq20$, $20<x\leq30$, . . ., $90<x\leq100$, respectively. Images were then broken into nonoverlapping tiles of $100 \times 100$ pixels.

To calculate HER2 ICD, HER2 ECD, and CD8 enrichment per tile, a cut-point of top 5% was selected for the original HER2 ICD and ECD signals, and 1% for the original CD8 signal, or given value "0" otherwise. HER2 ICD and ECD enrichment corresponded to the quotient of the number of pixels in a perimeter with ICD or ECD scores in top 5% over the number of pixels in the perimeter. CD8 enrichment was obtained from the quotient of the number of pixels in each envelope with CD8 scores in top 1% over the total number of pixels in that envelope. Because we are only interested in tumor regions with high expression levels of HER2 ICD, tiles with ICD values below the median were filtered out. The remaining tiles (those above the median ICD value) were split into ECD enrichment-low and -high groups using a median cut-point.

### Pairwise correlation matrix

Data from 18 markers were denoised and averaged to create $40 \times 40$ nonoverlapping tiles. We then partition the slides into $25 \times 25$ pixel nonoverlapping tiles and average the value for each marker in each tile. Because each image comprises $1{,}000 \times 1{,}000$ pixels and each tile comprises $25 \times 25$ pixels, we get (for each patient and each marker) a $40 \times 40$ tile image corresponding to a low resolution version of the original marker image.

## Results

Figure 1 shows raw ion images for 18 markers in a representative $HER2^+$ breast cancer case using MCD Viewer Software (v 1.0.554.0, Fluidigm). Pixel resolution was approximately at the 1 $\mu m^2$ level. Initially, we validated the IMC method to determine whether this method showed results similar to previously described results obtained by QIF (5). A direct comparison

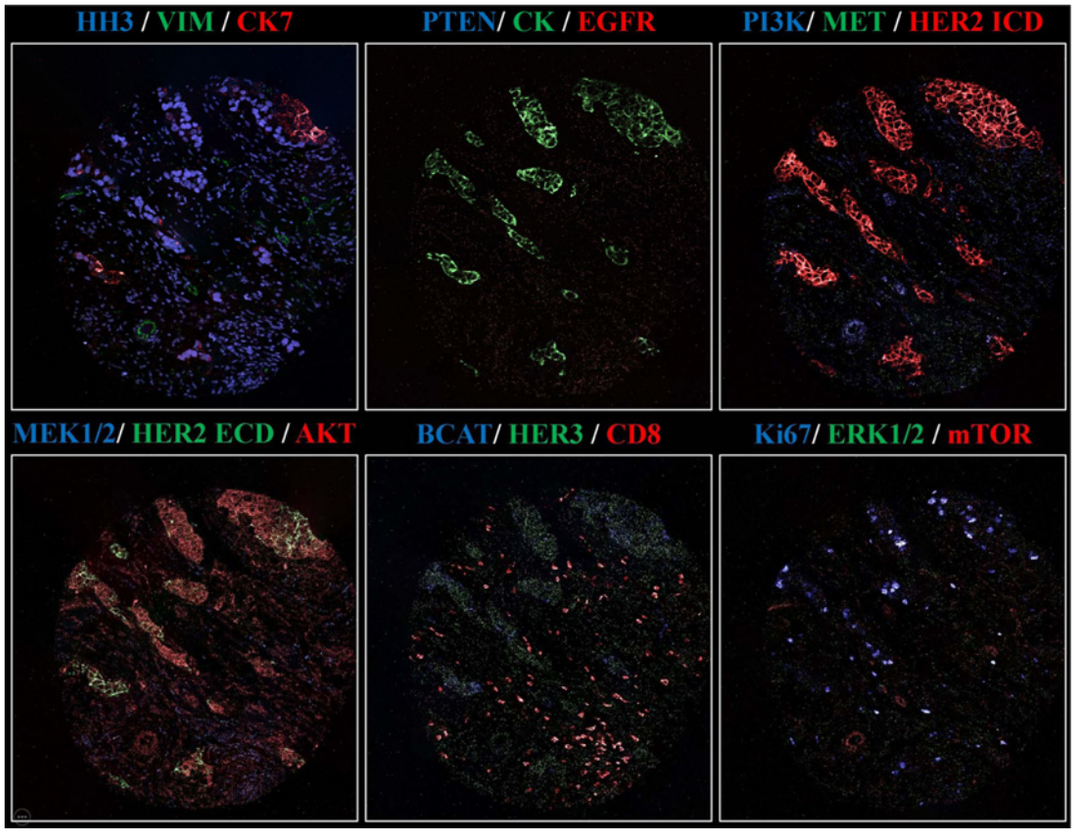


**Figure 1.**
Multiplexed detection of 18 protein targets using FFPE tissues and IMC. Pseudo-colored raw ion images representing the markers detected in the study.

is shown in two parts. First, data obtained using a HER2 standardization TMA showed that IMC is capable of correctly stratifying HER2 ICD levels into bins defined by the clinical assessment of each case as HER2-negative (IHC = 0 or 1) and -positive (IHC = 2 or 3; Fig. 2A). Then QIF results from different histospots of the same cases were compared with IMC (Fig. 2B). Good concordance is seen, but QIF has less dynamic range than IMC and appears to be saturated. The data were fit to logarithmic curve and showed high correlation ($r = 0.79$), similar to that seen by our group when chromogenic IHC was compared with QIF (5).

While orthogonal validation against other tests is good, the best validation of a new technology is against outcome. Because we have previously showed that the decreased ECD is associated with worse outcome in the HeCOG cohort (5) this provides a good cohort for validation of IMC. Here, we used a case–control series subset of $HER2^{+}$, trastuzumab-treated patients including 19 recurrent and 41 control cases selected from a larger cohort with the goal of validating the IMC technology against previously proven outcome (5). In this cohort, the presence of high levels of both ECD and ICD showed benefit from trastuzumab where those cases with high ICD but less ECD showed diminished benefit. To determine whether we could see similar effects with IMC, we assessed HER2 ECD and ICD levels using separately labeled antibody in a compartment defined by positive cytokeratin. We found that ICD- and ECD-high cases (defined by median cut-point) showed a trend toward decreased number of recurrences ($P = 0.057$; Fig. 3A). Patients with an elevated ECD/ICD intensity ratio in cytokeratin-positive compartment were significantly associated with lower number of 5-year recurrences ($P = 0.044$; Fig. 3B). This case–control series is underpowered for survival but shows a trend for better 5-year disease-free survival (log-rank $P = 0.066$; Fig. 3C) supporting validation of the IMC method.

For each slide, we calculated the correlations between every pair of markers. Each marker is represented by a vector with 1,600 values, corresponding to the intensities of the marker in the 40 × 40 tiles. A subset of all pairwise correlations corresponding to key pairs of structural and kinase signaling markers are displayed for 60 patients (Fig. 4). To determine the value of high-plex assessment of 17 markers we explored our data for correlations, both between markers and between the spatial arrangements of each marker. To study how correlations of these markers vary as a function of HER2 ECD richness, we sorted the columns in the heatmap which correspond to the 60 slides based on the total level of HER2 ECD normalized by the total level of CK7. As shown in the heatmap, higher correlation coefficients were consistently obtained for targets present in the same subcellular compartments (e.g., HER2 ICD and ECD, both domains of HER2 and CK7, and Histone H3 and Ki67). The inverse was also seen, with lower correlation for PI3K and Ki67, and HER2 and CD8, providing validation for our method that does not use cell boundaries for definition of event. Interestingly, we did not detect a pattern for positive correlation of either HER2 ICD or ECD with EGFR, HER3 or with known signaling partners, such as PI3K, ERK, and MEK,

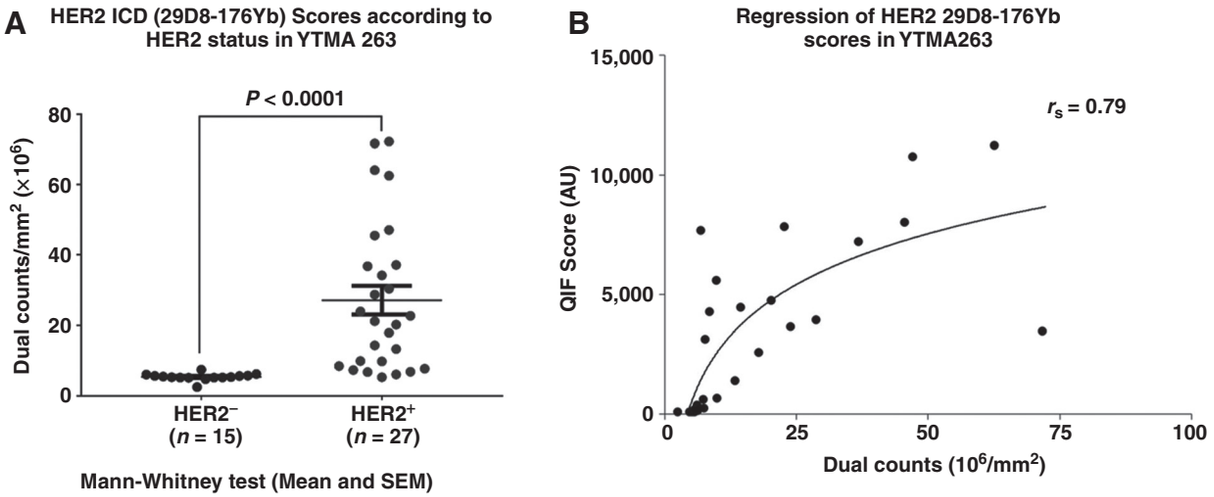


**Figure 2.**

HER2 measurement using IMC can classify clinical cases and is associated with QIF readings. **A,** HER2 ICD detected in denoised cytokeratin pixels correctly stratifies cases from a HER2 standardization array into predictive categories (Mann–Whitney test). **B,** HER2 ICD measured by IMC and QIF is positively associated and follows a logarithmic curve (*r*, correlation coefficient).

except for AKT. This may be due to our inability to assess phosphorylation status in these markers using the current antibody cocktail.

Finally, we generated an algorithm to search for meaningful spatial relationships between the markers. Because the majority of markers are colocalized in tumor cells, spatial relationships are beyond the resolution of the technology. However, the IMC approach allows us to determine the distribution patterns of T-cell infiltrates in a $HER2^+$ population with known distributions of ECD versus ICD. Figure 5A shows a representative schematic of the method used to define edge of tumor (see Materials and Methods). Perimeters of tumor islands were defined by thresholded HER2 ICD levels with a 100 × 100 resolution. Then $CD8^+$ tiles were evaluated as a function of fixed 10-μm contours around the perimeters and data were stratified for HER2 ECD in low and high groups using the median cut-point. Figure 5B depicts a single case illustrating that the mean CD8 fraction is higher in the ECD-high tiles compared with the ECD-low tiles, but that this relationship degrades with distance from the interface of tumor and stroma (the shoreline). When all 60 patients were analyzed (Fig. 5C), we observed significantly elevated CD8 levels close to the tumor stromal interface that again degrades with distance when assessing HER2 ECD–high tiles from all cases compared with low ECD tiles from all cases. This observation suggests that the CD8 distribution is significantly related to the HER2 ECD presence in the tumor cells and that this relationship degrades with distance from the tumor edge.

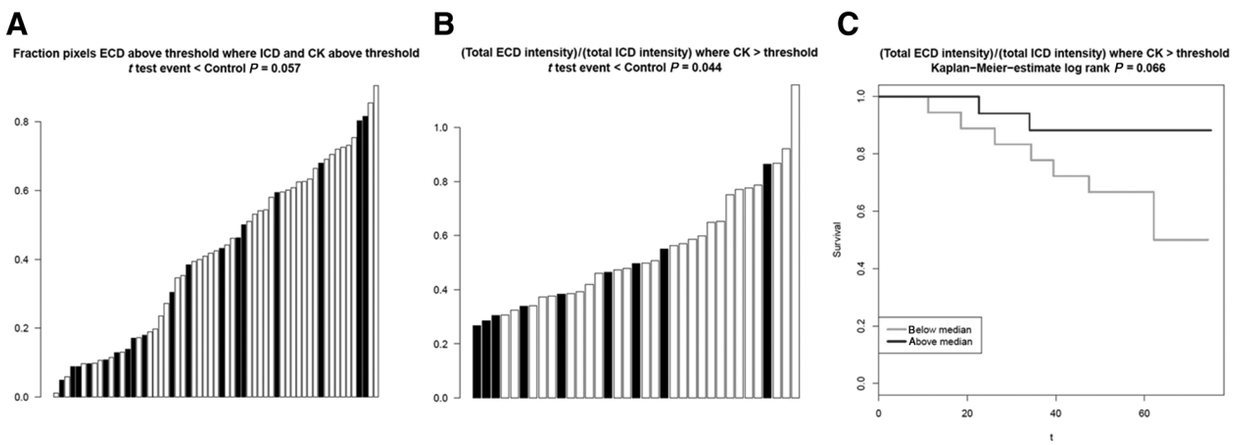


**Figure 3.**

Analysis of recurrence status in trastuzumab-treated patients using HER2 ECD/ICD measurement. **A,** Each case is shown on the *x* axis, ordered by fraction pixels positive for ECD when ICD and CK are over threshold (readable spots). The filled bars are patients that recurred after treatment with trastuzumab within 5 years. **B,** Similar to **A**, the *x* axis shows each patient ordered by ratio of ECD/ICD intensity showing recurrences in filled bars. **C,** Disease-free survival analysis stratified by HER2 ECD/ICD status.

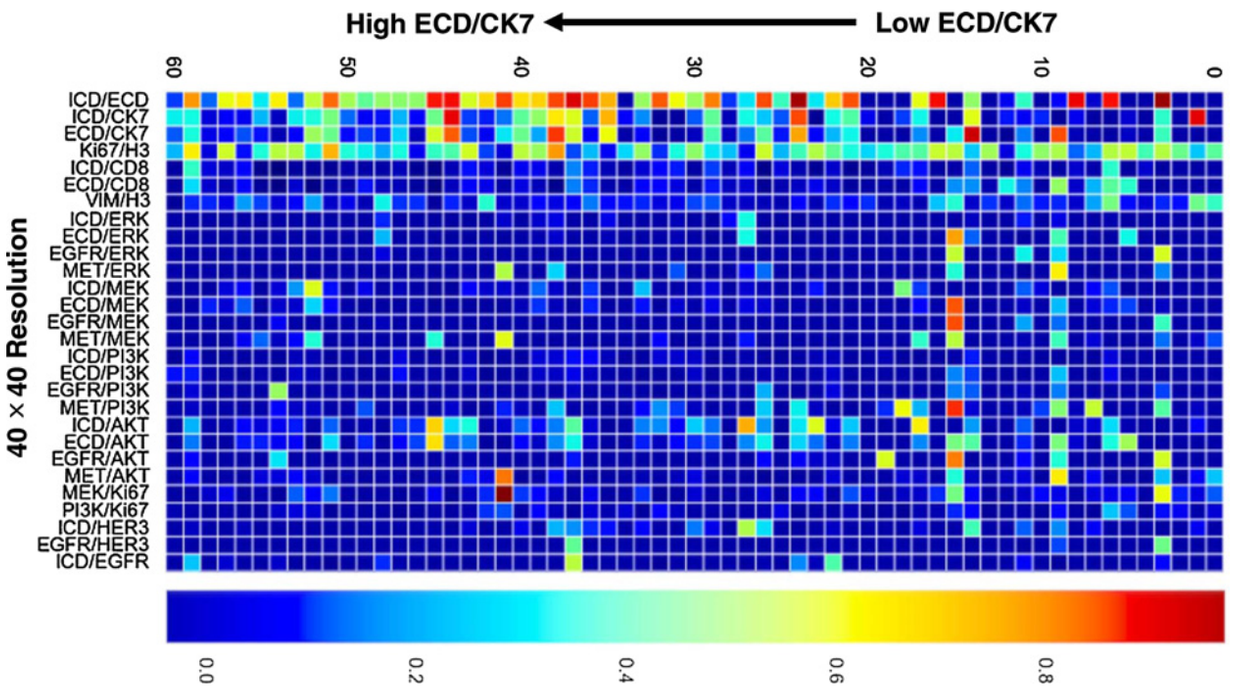


**Figure 4.**

Pairwise correlations for targets of interest across 60 trastuzumab-treated patients. Consistent association of targets within subcellular compartments and presence of the inverse pattern are present and validate a strategy using molecular-guided spatial analysis. A method based on cell segmentation could be more informative on signaling than a strict colocalization strategy. Color code shows strength of correlation (*r* value) when cases are sorted on the basis of ECD abundance over $CK7^+$ pixels.

## Discussion

IMC is among the new technologies capable of high-fold multiplexing, but still early in development. The initial efforts in our group have validated the technology using comparison with conventional IHC and QIF and importantly, also to outcome. We showed that concurrent detection of HER2 ICD and ECD was associated with better outcome after adjuvant chemotherapy plus trastuzumab than that seen in patients with decreased ECD. With this validation complete we went on to assess correlations between signaling molecules in the same cohort. Using a strategy that combines both number of molecular counts and their localization, we observed a relationship between CD8 expressed on cytotoxic T cells and the HER2 ECD that is not present for the ICD and is a function of close proximity. This observation provides new direct evidence of a more prominent or effective cytotoxic T-cell responses in ECD-high cases.

Initially our goal with this technology was to multiplex both the ECD and ICD of HER2 to allow construction of a ratio. Previous efforts to generate a ratio using multiplexed fluorescence were ineffective due to our inability to normalize for the variable quantum yield between fluorophores. For IMC, the metals detected by mass spectroscopy, although different in molecular weight, are counted with equal efficiency, allowing calculation of a ratio of the ECD and ICD in the same tissue, as opposed to serial sections, as described previously (5). Although serial section multiplexing predicted outcome, simultaneous measurement and calculation of a ratio of the domains both confirms the original observation and extends the hypothesis by showing increased predictive value of the ratio compared with ECD alone (Fig. 3).

Another novel finding achievable only using IMC data was the absence of correlation between HER2 ICD and EGFR and HER3. Both EGFR and HER3 have been shown to heterodimerize with HER2, and heterodimers have the potential to behave differently than homodimers of HER2. EGFR has been reported as overexpressed in 24%–48% of $HER2^+$ tumors by IHC (25–27). In addition, it has been shown that its expression might be associated with poor disease-free and overall survival after adjuvant, and metastatic trastuzumab treatment (26, 27). In the case of HER3, its presence has been observed in 27%–50% of $HER2^+$ patients (25–27) and linked to decreased progression-free survival after taxane plus trastuzumab (27, 28). However, using IMC, where all the antibodies are assessed simultaneously, the frequency of either heterodimerization event appears to be very low by this method of spatial fractionation. While it is hard to prove absence of an interaction, this data from actual breast cancers does not support the previous suggestions of the impact of heterodimerization seen in preclinical models. IMC assessment, at a $40 \times 40$ pixel resolution, also shows a trend for positive correlation between both domains of HER2 and AKT, but not with ERK, MEK, and PI3K, even though these targets are known signaling elements of the ERBB family of receptors (29). Because, in this first study, low sensitivity may limit the accuracy of this finding, further validation is needed for both of the above hypotheses related to tyrosine kinase signaling, IMC appears to uniquely reveal relationships not previously seen using conventional *in situ* assessment methods.

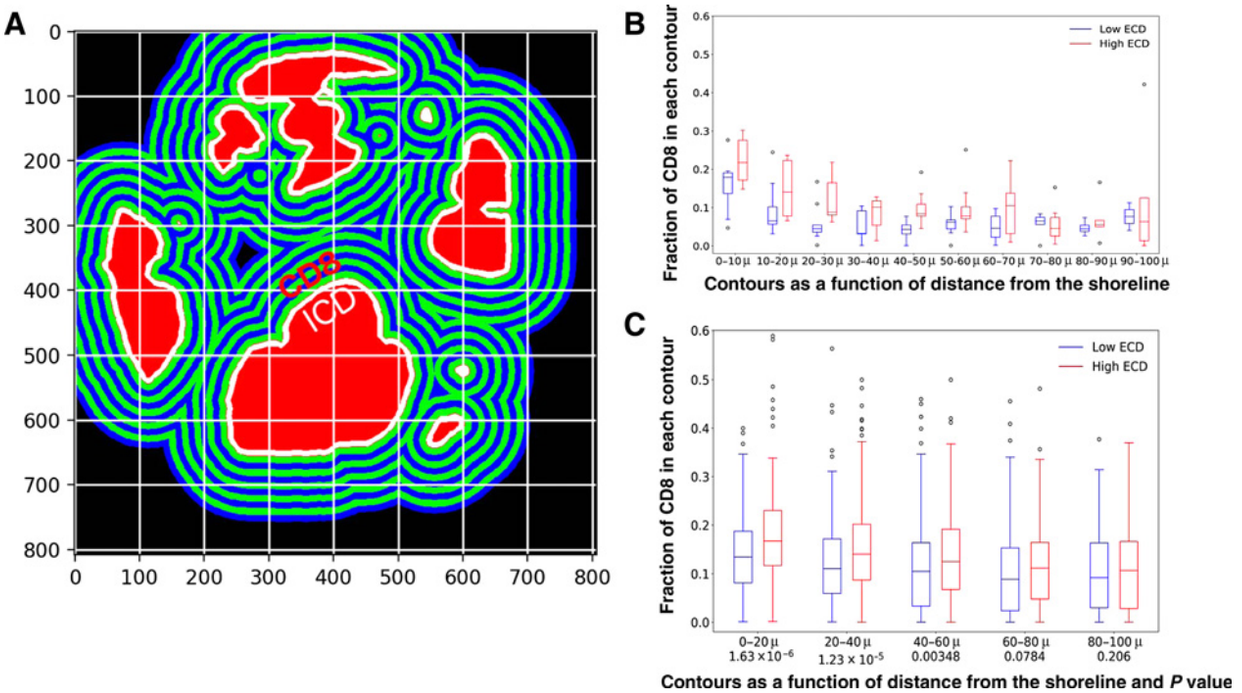


**Figure 5.**

T-cell cytotoxic infiltration as a function of distance from tumor envelopes and HER2 ECD levels. **A,** Shoreline method; "Geographic" analysis of spatial distribution using quantitative, objective measurement. Borders of HER2 ICD$^+$ islands are determined and distance intervals engulfing these islands are examined for abundance of a given marker (in this case, CD8). Data can be stratified later on the basis of other measurements, like HER2 ECD. **B,** In 2 representative patients, CD8 levels are elevated at close distance from the tumor (defined by HER2 ICD levels greater than a threshold) if HER2 ECD levels are also elevated at the tumor boundary. **C,** At a population level, cytotoxic T-cell infiltrates are significantly higher up to 60 μm from tumor in HER2 ECD–high patients, suggesting a HER2-driven adaptive immune component.

Perhaps the most interesting observation for this IMC study is the relationship between the ECD of HER2 and CD8. HER2$^+$ breast cancer has been associated with increased cytotoxic T-cell infiltration (30, 31). Within this subtype, increased tumor-infiltrating lymphocytes have a prognostic value and are linked to increased rates of pathologic complete response after neoadjuvant-targeted treatment with trastuzumab, lapatinib, or combination (30–32). This general observation has been used to indirectly support the role of ADCC in response to trastuzumab. Using a novel approach for spatial analysis using information on individual pixels and their distances rather than cell segmentation (33), we show that CD8-expressing cytotoxic T cells are found in close proximity to tumor cells with HER2 ECD with greater frequency than those more prominently expressing HER2 ICD. We also show diminution of this effect with distance, consistent with the proximity required for ADCC. This observation provides a potential explanation for the improved outcome seen in trastuzumab-treated patient with high tumor-infiltrating lymphocytes. Similarly, this is consistent with previous observations suggesting that the presence of p95HER2 (4, 34) might play a role in decreasing the adaptive antitumor response in HER2$^+$ breast cancer.

While our study is quantitative and includes response to treatment information, it has a number of limitations. First, the use of TMAs can underestimate or overestimate biomarker levels due to tumor heterogeneity. Ultimately, these observations will need to be validated on conventional whole tissue sections. Second, due to the relatively slow data collection process, our series is a pilot study, limited to a small, selected population of 19 recurrent and 41 control patients. Future studies are planned to include larger cohorts and prospectively collected tissues. Another limitation is our inability to assess the role of natural killer (NK) cells. While these cells are an important subset and could play a role in the response, we were unable to validate and label NK markers in this early biomarker panel.

In summary, objective measurement of HER2 ECD/ICD, signaling targets, and CD8 using IMC delivers information that might help identify patients that will derive benefit from targeted treatment or immunotherapy. While the use of IMC in the clinical setting is not immediately very likely, the IMC-derived discoveries could be converted into clinical tests including a proximity assay for CD8 and ECD and possibly an ECD/ICD ratio test, both toward to goal of more accurately predicting response to trastuzumab and related HER2 axis therapies. In addition, our study describes a method for spatial analysis of molecular abundance that does not require cell segmentation. We hope this work will support future efforts on understanding intracellular signaling and the tumor microenvironment using these highly multiplexed tools on patient tissues.

## Disclosure of Potential Conflicts of Interest

G. Foutzilas reports receiving speakers bureau honoraria from AstraZeneca and is a consultant/advisory board member for Pfizer, Sanofi, and Roche. K.A. Schalper reports receiving speakers bureau honoraria from Merck; is a consultant/advisory board member for Celgene, Moderna Inc., Shattuck Labs, and

Pierre Fabre; and reports receiving commercial research grants from Navigate BioPharma, Vasculox/Tioma, Tesaro, Moderna Inc., Surface Oncology, Pierre-Fabre Research Institute, Merck, and Bristol-Myers Squibb. Y. Kluger is a consultant/advisory board member for Corvus, Nektar, Biodesix, Genetech, Pfizer, Merck, and Celldex; and reports receiving commercial research support from Merck, Apexigen, and Bristol-Myers Squibb. D.L. Rimm is a consultant/advisory board member for Cell Signaling Technology, NanoString, and Agendia; and reports receiving commercial research grants from Navigate Biopharma, Perkin Elmer, and Ultivue. No potential conflicts of interest were disclosed by the other authors.

## Authors' Contributions

**Conception and design:** D.E. Carvajal-Hausdorf, Y. Kluger, D.L. Rimm
**Development of methodology:** D.E. Carvajal-Hausdorf, F. Villarroel-Espindola, R.R. Montgomery, K.A. Schalper, Y. Kluger, D.L. Rimm
**Acquisition of data (provided animals, acquired and managed patients, provided facilities, etc.):** D.E. Carvajal-Hausdorf, R.R. Montgomery, A. Psyrri, G. Foutzilas
**Analysis and interpretation of data (e.g., statistical analysis, biostatistics, computational analysis):** D.E. Carvajal-Hausdorf, J. Patsenker, K.P. Stanton, F. Villarroel-Espindola, A. Psyrri, Y. Kluger, D.L. Rimm
**Writing, review, and/or revision of the manuscript:** D.E. Carvajal-Hausdorf, J. Patsenker, F. Villarroel-Espindola, R.R. Montgomery, A. Psyrri, K.T. Kalogeras, V. Kotoula, G. Foutzilas, K.A. Schalper, Y. Kluger, D.L. Rimm
**Administrative, technical, or material support (i.e., reporting or organizing data, constructing databases):** D.E. Carvajal-Hausdorf, F. Villarroel-Espindola, A. Esch, V. Kotoula, K.A. Schalper, D.L. Rimm
**Study supervision:** Y. Kluger, D.L. Rimm

## Acknowledgments

This work was supported by the Breast Cancer Research Foundation, the NCI 554 (P30-CA016359), the Yale Cancer Center, (to D.L. Rimm), and the Hellenic Cooperative Oncology Group (to G. Foutzilas).

The costs of publication of this article were defrayed in part by the payment of page charges. This article must therefore be hereby marked *advertisement* in accordance with 18 U.S.C. Section 1734 solely to indicate this fact.

Received August 10, 2018; revised December 9, 2018; accepted February 8, 2019; published first February 22, 2019.

## References

1. Hudis CA. Trastuzumab–mechanism of action and use in clinical practice. N Engl J Med 2007;357:39–51.
2. Weiner LM, Adams GP. New approaches to antibody therapy. Oncogene 2000;19:6144–51.
3. Clynes RA, Towers TL, Presta LG, Ravetch JV. Inhibitory Fc receptors modulate *in vivo* cytotoxicity against tumor targets. Nat Med 2000;6:443–6.
4. Scaltriti M, Rojo F, Ocaña A, Anido J, Guzman M, Cortes J, et al. Expression of p95HER2, a truncated form of the HER2 receptor, and response to anti-HER2 therapies in breast cancer. J Natl Cancer Inst 2007;99:628–38.
5. Carvajal-Hausdorf DE, Schalper KA, Pusztai L, Psyrri A, Kalogeras KT, Kotoula V, et al. Measurement of domain-specific HER2 (ERBB2) expression may classify benefit from trastuzumab in breast cancer. J Natl Cancer Inst 2015;107:djv136.
6. Rimm DL, Carvajal-Hausdorf DE, Harbeck N, Fumagalli D, Rodrik-Outmezguine V, de la Pena L, de Azambuja E, et al. Low levels of HER2 extracellular domain (ECD) compared to intracellular domain (ICD) in NeoALTTO may segregate benefit from lapatinib and trastuzumab in breast cancer. Can Res 2018;78. Issue 4 Supplement.
7. Piccart-Gebhart M, Holmes E, Baselga J, de Azambuja E, Dueck AC, Viale G, et al. Adjuvant lapatinib and trastuzumab for early human epidermal growth factor receptor 2-positive breast cancer: results from the randomized phase iii adjuvant lapatinib and/or trastuzumab treatment optimization trial. J Clin Oncol 2016;34:1034–42.
8. Hammond ME, Hayes DF, Dowsett M, Allred DC, Hagerty KL, Badve S, et al. American Society of Clinical Oncology/College of American Pathologists guideline recommendations for immunohistochemical testing of estrogen and progesterone receptors in breast cancer. J Clin Oncol 2010;28:2784–95.
9. Wolff AC, Hammond ME, Hicks DG, Dowsett M, McShane LM, Allison KH, et al. Recommendations for human epidermal growth factor receptor 2 testing in breast cancer: American Society of Clinical Oncology/College of American Pathologists clinical practice guideline update. J Clin Oncol 2013;31:3997–4013.
10. Rimm DL, Han G, Taube JM, Yi ES, Bridge JA, Flieder DB, et al. A prospective, multi-institutional, pathologist-based assessment of 4 immunohistochemistry assays for PD-L1 expression in non-small cell lung cancer. JAMA Oncol 2017;3:1051–8.
11. Brown JR, Wimberly H, Lannin DR, Nixon C, Rimm DL, Bossuyt V. Multiplexed quantitative analysis of CD3, CD8, and CD20 predicts response to neoadjuvant chemotherapy in breast cancer. Clin Cancer Res 2014;20:5995–6005.
12. Feng Z, Puri S, Moudgil T, Wood W, Hoyt CC, Wang C, et al. Multispectral imaging of formalin-fixed tissue predicts ability to generate tumor-infiltrating lymphocytes from melanoma. J Immunother Cancer 2015;3:47.
13. Parra ER, Uraoka N, Jiang M, Cook P, Gibbons D, Forget MA, et al. Validation of multiplex immunofluorescence panels using multispectral microscopy for immune-profiling of formalin-fixed and paraffin-embedded human tumor tissues. Sci Rep 2017;7:13380.
14. Gerdes MJ, Sevinsky CJ, Sood A, Adak S, Bello MO, Bordwell A, et al. Highly multiplexed single-cell analysis of formalin-fixed, paraffin-embedded cancer tissue. Proc Natl Acad Sci U S A 2013;110:11982–7.
15. Lin JR, Izar B, Wang S, Yapp C, Mei S, Shah PM, et al. Highly multiplexed immunofluorescence imaging of human tissues and tumors using t-CyCIF and conventional optical microscopes. Elife 2018;7:e31657.
16. Giesen C, Wang HA, Schapiro D, Zivanovic N, Jacobs A, Hattendorf B, et al. Highly multiplexed imaging of tumor tissues with subcellular resolution by mass cytometry. Nat Methods 2014;11:417–22.
17. Angelo M, Bendall SC, Finck R, Hale MB, Hitzman C, Borowsky AD, et al. Multiplexed ion beam imaging of human breast tumors. Nat Med 2014;20:436–42.
18. Schapiro D, Jackson HW, Raghuraman S, Fischer JR, Zanotelli VRT, Schulz D, et al. histoCAT: analysis of cell phenotypes and interactions in multiplex image cytometry data. Nat Methods 2017;14:873–6.
19. Camp RL, Chung GG, Rimm DL. Automated subcellular localization and quantification of protein expression in tissue microarrays. Nat Med 2002;8:1323–7.
20. Neumeister VM, Anagnostou V, Siddiqui S, England AM, Zarrella ER, Vassilakopoulou M, et al. Quantitative assessment of effect of preanalytic cold ischemic time on protein expression in breast cancer tissues. J Natl Cancer Inst 2012;104:1815–24.
21. Gustavson MD, Rimm DL, Dolled-Filhart M. Tissue microarrays: leaping the gap between research and clinical adoption. Per Med 2013;10:441–51.
22. Bordeaux J, Welsh AW, Agarwal S, Killiam E, Baquero MT, Hanna JA, et al. Antibody validation. Biotechniques 2010;48:197–209.
23. Uhlen M, Bandrowski A, Carr S, Edwards A, Ellenberg J, Lundberg E, et al. A proposal for validation of antibodies. Nat Methods 2016;13:823–7.
24. Fountzilas G, Dafni U, Papadimitriou C, Timotheadou E, Gogas H, Eleftheraki AG, et al. Dose-dense sequential adjuvant chemotherapy followed, as indicated, by trastuzumab for one year in patients with early breast cancer: first report at 5-year median follow-up of a Hellenic Cooperative Oncology Group randomized phase III trial. BMC Cancer 2014;14:515.
25. Abd El-Rehim DM, Pinder SE, Paish CE, Bell JA, Rampaul RS, Blamey RW, et al. Expression and co-expression of the members of the epidermal growth factor receptor (EGFR) family in invasive breast carcinoma. Br J Cancer 2004;91:1532–42.
26. Lee HJ, Seo AN, Kim EJ, Jang MH, Kim YJ, Kim JH, et al. Prognostic and predictive values of EGFR overexpression and EGFR copy number alteration in HER2-positive breast cancer. Br J Cancer 2015;112:103–11.

27. Park YH, Jung HA, Choi MK, Chang W, Choi YL, Do IG, et al. Role of HER3 expression and PTEN loss in patients with HER2-overexpressing metastatic breast cancer (MBC) who received taxane plus trastuzumab treatment. Br J Cancer 2014;110:384–91.
28. Lipton A, Goodman L, Leitzel K, Cook J, Sperinde J, Haddad M, et al. HER3, p95HER2, and HER2 protein expression levels define multiple subtypes of HER2-positive metastatic breast cancer. Breast Cancer Res Treat 2013;141: 43–53.
29. Yarden Y, Sliwkowski MX. Untangling the ErbB signalling network. Nat Rev Mol Cell Biol 2001;2:127–37.
30. Mahmoud SM, Paish EC, Powe DG, Macmillan RD, Grainge MJ, Lee AH, et al. Tumor-infiltrating CD8+ lymphocytes predict clinical outcome in breast cancer. J Clin Oncol 2011;29:1949–55.
31. Ali HR, Provenzano E, Dawson SJ, Blows FM, Liu B, Shah M, et al. Association between CD8+ T-cell infiltration and breast cancer survival in 12,439 patients. Ann Oncol 2014;25:1536–43.
32. Salgado R, Denkert C, Demaria S, Sirtaine N, Klauschen F, Pruneri G, et al. The evaluation of tumor-infiltrating lymphocytes (TILs) in breast cancer: recommendations by an International TILs Working Group 2014. Ann Oncol 2015;26:259–71.
33. Al-Kofahi Y, Lassoued W, Lee W, Roysam B. Improved automatic detection and segmentation of cell nuclei in histopathology images. IEEE Trans Biomed Eng 2010;57:841–52.
34. Anido J, Scaltriti M, Bech Serra JJ, Santiago Josefat B, Todo FR, Baselga J, et al. Biosynthesis of tumorigenic HER2 C-terminal fragments by alternative initiation of translation. EMBO J 2006;25:3234–44.